Engineering soil barriers to minimise annual shrinkage/swelling in plastic clays

Aikaterini Tsiampousi [a,*], Charlotte Day [a], Alexandros Petalas [b]

[a] *Imperial College London, Department of Civil & Environmental Engineering, London, UK*
[b] *University of Durham, Department of Civil Engineering, Durham, UK*

A B S T R A C T

Engineered soil barriers have been proposed to prevent rainwater infiltration into the underlying soil, thus improving stability of sloping ground. The use of engineered barriers on flat ground as means of preventing flooding has also been explored. This paper aims to provide proof-of-concept as to the potential efficiency of engineered barriers in minimising soil shrinkage and swelling arising from seasonal variations of water content and pore water pressures within the ground due to its interaction with the atmosphere. A series of 2-dimensional, hydro-mechanically coupled finite element analyses were conducted to this effect. Emphasis was placed on accurately modelling the stiffness of the underlying soil, accounting for its small-strain behaviour, as well as the hydraulic behaviour of all the layers involved. The results confirm that it is possible to engineer barriers to minimise shrinkage/swelling in greenfield, as well as urban, conditions and highlight the influence of barrier geometry and configuration, so that recommendations for the design of such barriers can be made.

1. Introduction

Climate change, associated with increasingly dry summers and wet winters,[9] alongside increasing urbanisation,[38] has not only led to a greater incidence of flooding but also of significant shrinkage/swelling which threatens infrastructure. Swelling arises in fine-grained soils absorbing rainfall water, while shrinkage occurs when these soils dry under warm and dry periods.[11] The associated volume changes depend on changes in porosity and water content of the clay,[5] alongside clay minerology, fabric, and dry density.[19] Shrinkage and swelling are responsible for subsidence of buildings and differential settlements[12] and have worsened in recent years, as evidenced by the increased frequency of insurance claim surges due to soil subsidence since the 1970s[25]. The phenomenon is anticipated to worsen further with climate change,[8] which is expected to result in greater annual soil water content variability. Harrison et al.[8] found that under a high emissions climate change scenario, 100% of clay rich areas would be at an increased susceptibility for shrinkage/swelling by 2080, which invariably would lead to more residential areas being impacted by serviceability problems.

One proposed engineered solution is to design and optimise soil barriers which minimise the percolation and evaporation of water to and from the ground, and therefore water content fluctuations in underlying soil and by extension shrinkage and swelling. A significant body of relevant work was recently produced by collaborators in the Climate Adaptation Control Technologies for Urban Spaces (CACTUS) project (e. g.,[13,3,13,34]). The proposed engineered barriers consist of two layers, a water holding and a drainage layer.

The purpose of the water holding layer is to accommodate and store rainfall water, and for this reason it is imperative that it has favourable water holding properties. Toll et al.[34] demonstrated that the addition of waste treatment residual (WTR) enhanced the water retention properties of soil, possibly by inducing beneficial changes to the soil fabric and introducing a larger proportion of fines. They compared two sandy loam control soils from Durham and Dundee to soils amended with 2%, 5% and 10% WTR and a co-amendment of 5% compost – 5% WTR. The water content of the co-amended soil was approximately double that of the corresponding control soil at 10 kPa suction. These findings were corroborated by Kerr et al.[13] who tested various single WTR and compost amendments, as well as WTR/compost co-amendments at various fractions and compared them to the same control soils, demonstrating that such amendments and co-amendments are appropriate candidates for the water holding layer.

The purpose of the drainage layer is to provide a capillary break.

---

* Correspondence to: London Department of Civil & Environmental Engineering, Skempton Building, London SW7 2AZ, UK.
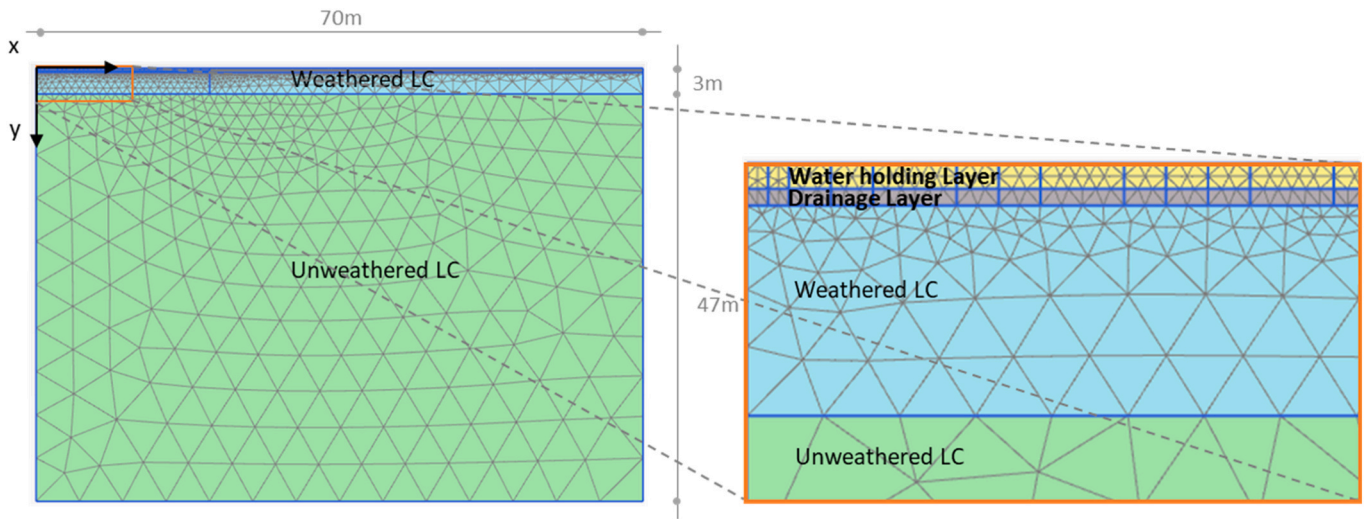*E-mail address:* aikaterini.tsiampousi@imperial.ac.uk (A. Tsiampousi).
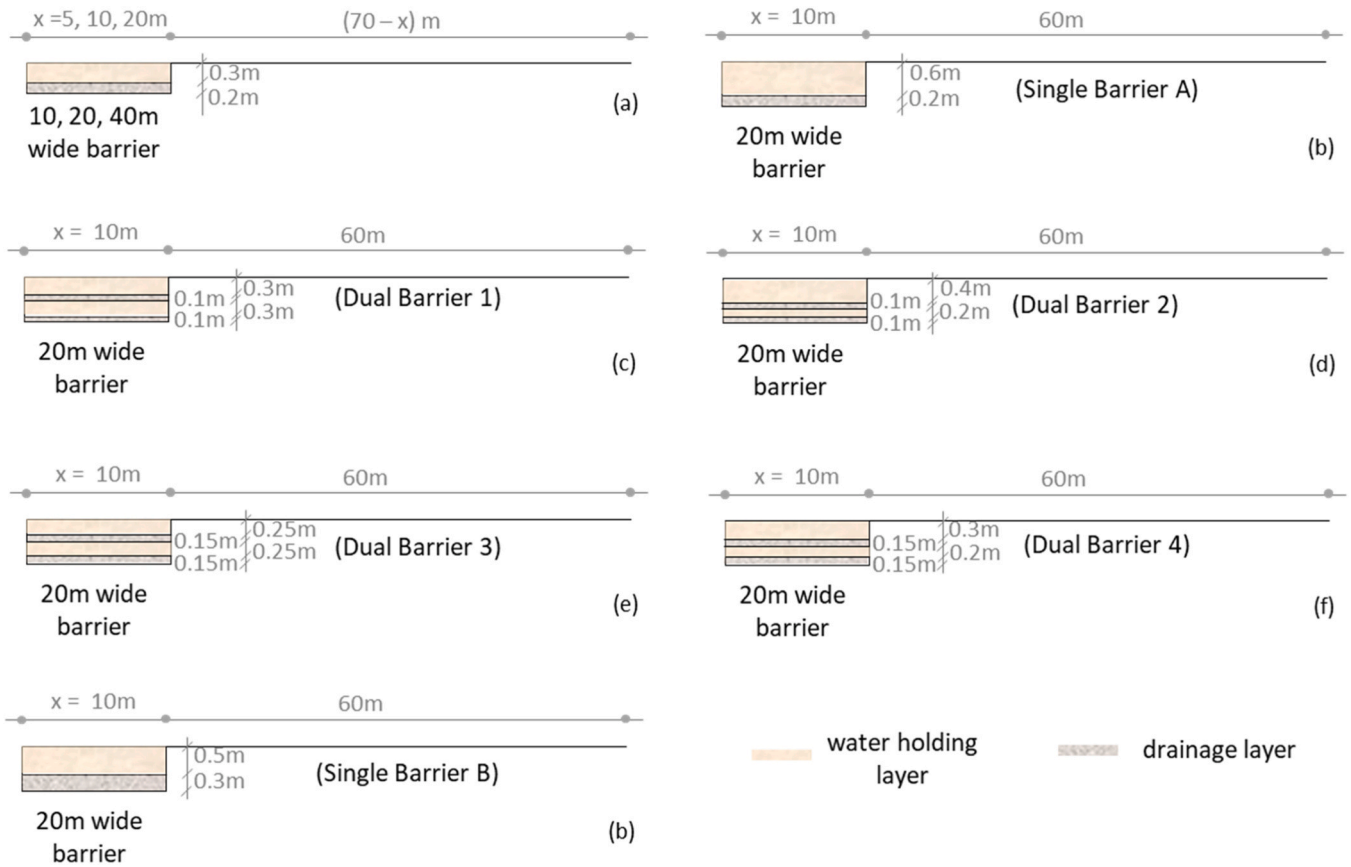
Fig. 1. Typical FE mesh.

Fig. 2. Geometries considered in greenfield conditions.

Capillary barriers arise in unsaturated conditions, where a fine-grained soil lies above a coarse-grained soil. The difference in soil hydraulic properties results in capillary tension, which supports water retention in the fine-grained layer until saturation increases to the point of break-through.[14] At breakthrough, flow of water through the bottom of the coarse layer is observed. Capillary barriers have been shown to reduce water content fluctuations in underlying soil (e.g.,[26]).

There has also been significant work done into how engineered barriers may be optimised to accommodate water storage, and prevent flooding. Parent and Cabral[23] concluded that effective barriers require

high maximum suction and hydraulic conductivity in the water holding layer and low maximum suction in the drainage layer. Furthermore, increasing the coarseness of the drainage layer relative to the water holding layer increases lateral diversion of water, delaying infiltration.[28] This is due to the water entry value decreasing as coarseness of the drainage layer increases.[41] Sensitivity analyses on engineered barriers conducted by Li et al.[16] demonstrated that as the thickness of the fine-grained layer increased, the water storage capacity of the engineered barrier was augmented. Petalas et al.[24] provided proof-of-concept through numerical analysis that engineered barriers
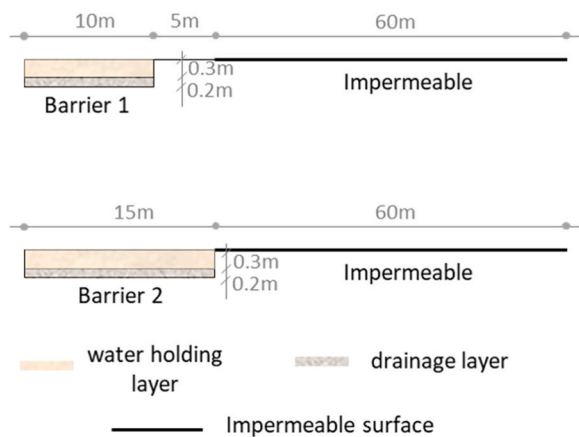
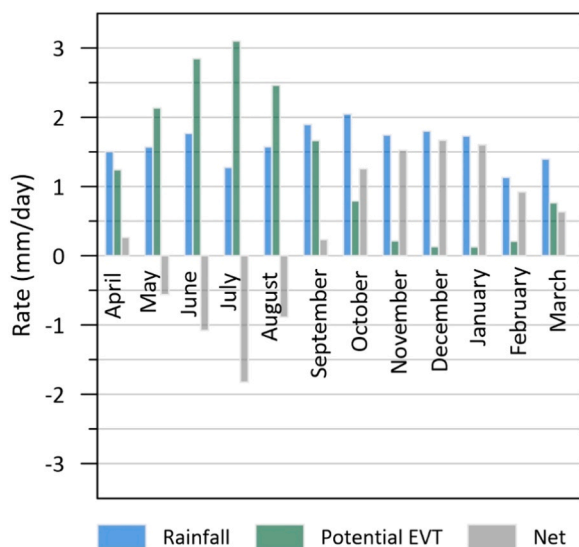Fig. 3. Geometries considered in urban conditions.

Fig. 4. Climatic data.

can prevent rainfall water run-off under infiltration intensities which induce run-off in the control soil.

Further improvements in the water holding capacity of capillary barriers can be made through adopting a dual capillary barrier (DCB) design with two fine-grained layers and two coarse-grained layers.[7] This conclusion is supported by the work of Scarfone et al.[27] who demonstrated the beneficial effect of employing a DCB on a slope under constant infiltration by preventing breakthrough.

The focus of previous research has been on the water holding capacity of engineered barriers and on their impact on water content and suction fluctuations in the underlying, in-situ soil. So far there has been little research done on the potential use of engineered barriers to minimise shrinkage/swelling in the in-situ soil. Petalas et al.[24] demonstrated in 1D numerical analyses that potentially significant gains can be made. The present paper explores this idea and examines how various geometrical factors, such as the barrier depth as well as its width, may impact on the annual shrinkage/swelling of a typical in-situ soil susceptible to large volumetric changes caused by water content fluctuations.

For this purpose, a well-studied geo-material, London clay, was considered as the in-situ soil. A water holding layer from the recent work of Kerr et al.[13] was selected and paired with a coarse-grained drainage layer[10] to form the engineered barrier. Series of 2D fully coupled finite element analyses were conducted with the Finite Element program

Plaxis 2D,[2] making use of bespoke, in-house developed, user-defined soil and flow models to reproduce the behaviour of the clay. Particular focus was placed on capturing the small-strain stiffness of the in-situ soil, where displacements were examined and where buried structures may exist and may be negatively impacted on by cyclic seasonal displacements. The paper aims to provide proof-of-concept as to the effective use and engineering of soil barriers to minimise the amplitude of shrinkage/swelling cycles caused by interaction of the soil with the atmosphere.

2. Problem definition

2.1. Geometry and cases considered

A typical stratigraphy with a 3 m deep layer of weathered London clay (LC), overlying 47 m of unweathered LC, was employed for the in-situ soil. Therefore, a 50 m deep and 140 m wide soil domain was considered in half symmetry (i.e. the numerical model was actually 70 m wide). A typical FE mesh is shown in Fig. 1. It was designed such that the FE elements were finer at the interface with the atmosphere, getting progressively coarser with depth. The bottom boundary coincided with the interface with the underlying chalk. The displacements within the in-situ soil were studied at various depths along the axis of symmetry, before and after the construction of the barrier. The ground surface was vegetated with shrubs, which were excavated with the soil and replaced when the barrier was constructed. The details of how soil-atmosphere interaction was modelled and of the analysis sequence are given in subsequent sections. The current section presents the different barrier geometries examined.

The effect of barrier width was investigated first considering a 0.5 m deep barrier, comprising a 0.3 m thick water holding layer and a 0.2 m thick drainage layer. Three different widths were examined: 10, 20 and 40 m (note that due to symmetry only half the width was simulated in each analysis). This is shown schematically in Fig. 2(a).

Subsequently, two depths were considered, both for the 20 m wide barrier. A 0.5 m deep barrier as above and a 0.8 m deep barrier, shown in Fig. 2(b), where the water holding layer was 0.6 m thick, leaving the drainage layer at 0.2 m thickness as before.

The effect of employing dual capillary break (DCB) barriers was also examined in a total of four analyses. In all cases, the total depth of the barrier was 0.8 m and the width was 20 m, as schematically shown in Fig. 2(c) to (f). The two drainage layers of each DCB barrier had the same thickness: 0.1 m in Dual Barriers 1 and 2, and 0.15 m in 3 and 4. To compare dual with single capillary barriers, two single barriers were investigated: the same 0.8 m thick barrier as above (i.e., comprising 0.6 m of water holding layer and 0.2 m of drainage layer, to be compared with Dual Barriers 1 and 2) and an additional 0.8 m thick barrier, comprising of 0.5 m of water holding layer and 0.3 m of drainage layer (Fig. 2(g)), to be compared with Dual Barriers 3 and 4. Dual Barriers 1 and 3 consisted of two water holding layers of equal thickness (0.3 and 0.25 m, respectively), while Dual Barriers 2 and 4 consisted of a thicker top and a thinner bottom water holding layer (0.4 and 0.2 m for Dual Barrier 2, and 0.3 and 0.2 m for Dual Barrier 4).

The analyses above refer to "greenfield" conditions, where the ground surface was permeable and interacting with the atmosphere without any restrictions, other than those arising from the soil permeability and its water holding capacity (see sections on soil properties and on boundary conditions). In a built, urban or rural, environment, it is unlikely that the ground surface is not partially covered in impermeable surfaces, such as concrete pavements, buildings etc. To simulate "urban" conditions in a simplified manner and explore the potential benefit of engineering barriers in built environments, two extra analyses were performed employing an impermeable boundary at part of the top boundary of the FE mesh, extending from 15 m from the axis of symmetry to the edge of the mesh (Fig. 3). In both cases, a 0.5 m deep barrier was considered. In Barrier 1, the width was 10 m, i.e. the barrier did not cover the whole of the "permeable" area capable of interacting with the

Table 1
Model parameters for weathered and unweathered London clay.

Strength parameters												
Angle of shearing resistance, φ' (degrees)					Cohesion, c' (kPa)					Angle of dilation, v (degrees)		
23°					7.0					0.0		
Small strain stiffness parameters												
G_0 (kPa)	K_0 (kPa)	G_{min} (kPa)	K_{min} (kPa)	m_G ()	m_k ()	a_0 ()	b ()	$R_{G,min}$ ()	$R_{k,min}$ ()	r_0 ()	s ()	
955	1665	2000	3000	0.7	0.7	1.81E-4	1.3	5E-2	7.9E-2	3E-4	1.1	
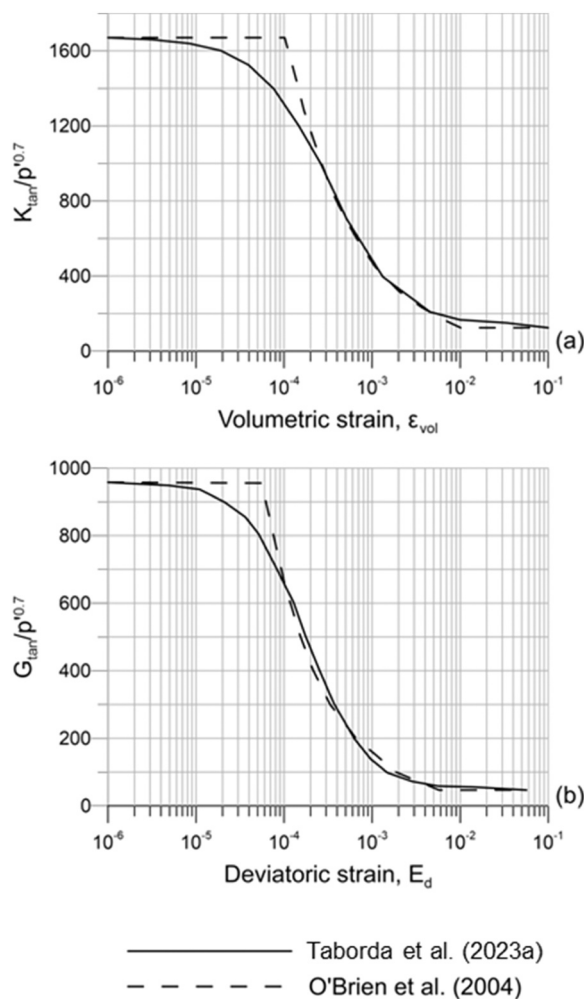
Fig. 5. Degradation of (a) Bulk stiffness with volumetric strain and (b) of Shear Stiffnesses with deviatoric strain
Adapted from[36]

atmosphere. In Barrier 2, the width was 15 m, covering the "permeable" area entirely.

2.2. Soil-atmosphere interaction

Soil-atmosphere interaction was modelled in PLAXIS 2D using the infiltration boundary condition, which is a dual boundary condition applied at the interface between the soil and the atmosphere and changing automatically from a user-defined pore water pressure (head) condition to an inflow/outflow condition with a user-defined rate and vice versa. Rainfall and evapotranspiration rates need to be combined into a single net inflow/outflow rate.

Average long-term monthly rainfall data were used in the analysis. They refer to Greenwich, London and were also used by Tsiampousi et al.[36] and Petalas et al.[24] They were combined with potential evapotranspiration (PET) data calculated by Tsiampousi et al.[36] for shrubs. The adopted rates are shown in Fig. 4.

The maximum possible head was set to 0 m (or 0kPa of pore water pressure), so that no suctions were maintained artificially within the ground, but ponding was avoided. The minimum possible head was set equal to − 150 m (or ~1500 kPa of suction), agreeing with previous values reported in the literature (e.g.,[21,35]).

2.3. Initial conditions and analysis sequence

Initially, only the in-situ soil (weathered and unweathered LC) was present in the FE mesh. The stresses were initialised at the very beginning of the analysis assuming for both layers a unit weight of 19.1 kN/m³. The groundwater table was at the ground surface and the initial pore water pressure distribution with depth was hydrostatic. The coefficient of earth pressure at rest K_0 was 2.1.

The analysis was fully coupled, simulating soil-atmosphere interaction for a total of 10 years, 5 before and 5 after the construction of the barrier. For the first 5 years, the atmospheric boundary conditions simulating the effect of rainfall and evapotranspiration from shrubs were applied everywhere at the top of the FE mesh. The same, average, climatic year (Fig. 4) was applied 5 successive times. The axis of symmetry and the right-hand-side vertical boundary of the mesh were impermeable, effectively simulating 1D flow conditions. The pore water pressure at the bottom boundary (interface with permeable chalk) was kept constant to its initial value, while the pore water pressures within the soil changed seasonally under the influence of the atmospheric boundary condition. This first part of the analysis enabled the study of displacements within the in-situ soil prior to the construction of the barrier.

In the second part of analysis, construction of the barrier was simulated in an undrained manner. First, the soil in the area where the barrier was to be constructed was excavated. Then, the drainage and water holding layers were constructed simultaneously with a unit weight of 20 kN/m³ and 19 kN/m³, respectively. Their degree of saturation was set to 80% and the corresponding suction was initialised automatically from the respective soil-water retention curve (see subsequent section).

Finally, the third, fully coupled, part of the analysis simulated 5 years of soil-atmosphere interaction after the construction of the barrier. The same inflow/outflow rates were applied as before, everywhere at the top boundary of the FE mesh. Although all other hydraulic boundary conditions were also identical to those before the barrier construction, flow conditions were no longer 1D due to the different hydraulic properties of the barrier in relation to the in-situ soil, and the fact that the barrier did not cover the whole width of the mesh. Evidence to support this are provided when discussing the results.

In the two analyses simulating urban conditions, the top boundary of the mesh from a distance of 15 m from the axis of symmetry until the edge of the mesh was considered fully impermeable throughout the analysis. The remaining area from the axis of symmetry until the 15 m mark was subject to soil-atmosphere interaction, as above, both before and after the construction of the barrier. Again, all other hydraulic boundary conditions were identical to previous analyses.

In all the analyses, the horizontal displacements were restricted at the axis of symmetry and the right-hand-side vertical boundary, while

Table 2
Permeability model parameters for London clay.

Unweathered London clay (Eq. 1)			
Vertical permeability at $p' = 0$ kPa, k_0 (m/s)	Coefficient, α ()		
$3.7 * 10^{-9}$	0.007		
Weathered London clay (Eq. 2)			
Vertical permeability when cracks are closed, k_0 (m/s)	Maximum vertical permeability, k_{max} (m/s)	Tensile total principal stress σ_{T1} (kPa)	Tensile total principal stress σ_{T2} (kPa)
$4.3 * 10^{-8}$	$4.3 * 10^{-6}$	0.0	100.0
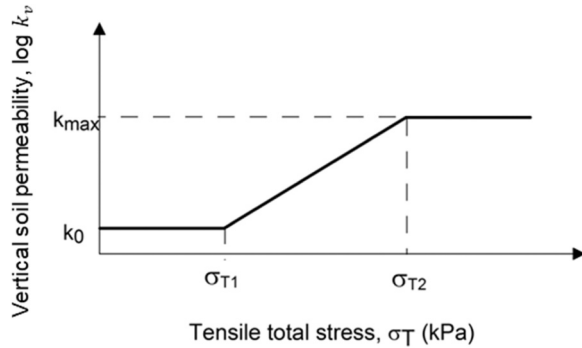
Fig. 6. Assumed variation of vertical soil permeability with suction Modified from[20].

both the horizontal and vertical displacements were restricted at the bottom boundary.

2.4. Material properties

2.4.1. In-situ soil

The mechanical behaviour of the in-situ LC was modelled with a constitutive model combining the Taborda et al.[30] small-strain stiffness model with the Mohr-Coulomb failure criterion. It was developed and implemented into PLAXIS 2D as a user-defined soil model by Taborda et al.[33,32] The model parameters (Table 1) were the same for the weathered and unweathered LC and had been calibrated by Tsiampousi et al.[36] and employed by Petalas et al.[24] Of particular interest is the degradation of bulk and shear stiffness, which is shown in Fig. 5 in comparison with curves from O'Brien.[22] The drained shear strength was calibrated on data from Kovacevic et al.[15] The model parameters are further explained in the Appendix.

The hydraulic behaviour of LC was modelled as fully saturated due to its high air-entry value of suction (e.g.[6]) which can be as high as 1 MPa, far exceeding the values of suction expected and achieved in the analysis. The values of saturated vertical permeability employed are summarised in Table 2 and are in agreement with values reported by Smethurst et al.[29] and previously employed by Tsiampousi et al.[36] and Petalas et al.[24] The vertical permeability, k_v, of the unweathered clay was modelled to reduce from its initial value k_0 with increasing mean effective stress, p', according to a fitting parameter a:

$$k_v = k_0 e^{ap'} \tag{1}$$

k_0 is the value of saturated vertical permeability at zero mean effective stress (Table 2). The value of 0.007 m²/kN, suggested by Kovacevic et al.,[15] was adopted for a. Due to the 2D nature of the water flow after the construction of the barrier, it was deemed important to account for permeability anisotropy in the unweathered LC. Various anisotropy ratios k_h/k_v (k_h being the horizontal permeability) have been suggested in the literature: 4 by Mair,[17] 2–10 by Wongsaroj et al.,[40] 2 by Avgerinos et al.[1] A ratio of 2 was adopted here. The vertical permeability

was updated first based on the current value of p', and the horizontal permeability was calculated subsequently in order to keep the ratio k_h/k_v equal to 2. The permeability model described here is not a standard feature of PLAXIS 2D and was implemented as a user-defined flow model by Bui et al.[4] and Taborda et al.[31]

Desiccation cracking during the dry, summer months when evapotranspiration prevails and large suctions may build up, can temporarily increase the mass permeability of the upper soil layer. Cracks are likely to close during wet, winter months, when rainfall prevails. A modification of the variable permeability model described in Nyambayo[20] was implemented into PLAXIS 2D as a user-defined flow model by Tsiampousi et al.,[37] to account for the seasonal variation of vertical permeability, k_v, due to desiccation cracks opening and closing:

$$\log k_v = \log k_{0,1} + \frac{\sigma_T - \sigma_{T1}}{\sigma_{T2} - \sigma_{T1}} \log\left(\frac{k_{max}}{k_{0,1}}\right) \tag{2}$$

where σ_T is the current tensile total principal stress and σ_{T1} and σ_{T2} define the total stress range, within which, the permeability is affected by desiccation cracking, as illustrated in Fig. 6. $k_{0,1}$ is the vertical permeability when the cracks are closed ($\sigma_T \leq \sigma_{T1}$) and k_{max} is the maximum possible vertical permeability when $\sigma_T \geq \sigma_{T2}$. The values of σ_{T1}, σ_{T2} and k_{max} used in the analysis are summarised in Table 2 and were adopted from Tsiampousi et al.[36] Whereas in the original model by Nyambayo[20] soil permeability was isotropic, the modification by Tsiampousi et al.[37] allows anisotropy by introducing an anisotropy ratio k_h/k_v. There are two options offered in the model: (a) the anisotropy ratio is kept constant, so that both vertical and horizontal permeabilities vary with desiccation cracking in a similar manner, or (b) the horizontal permeability remains unchanged and unaffected by desiccation cracking. The second option was adopted in the analyses, with an initial anisotropy ratio of 2. Desiccation cracking was considered only for the weathered and not for the unweathered LC, since cracks appear usually on the surface, and they do not exceed the three meters depth that was assumed for the weathered LC in this study.

2.4.2. Barrier

The water holding layer of the barrier was assumed to be derived from a sandy loam soil from Durham amened with 5% WTR and tested by Kerr et al.[13] Its measured soil-water retention curve (SWRC) is presented in Fig. 7(a), together with the modelled behaviour. Despite recognising the importance that hysteretic hydraulic behaviour has on the hydraulic response of the barrier, which was highlighted by Scarfone et al.,[27] given the lack of laboratory data on the hysteretic hydraulic behaviour of the amendment, it was decided that increasing the modelling complexity, as well as the modelling uncertainty, was not justified. A version of the monotonic van Genuchten[39] retention curve, which is readily available in PLAXIS 2D, was employed. Its equation is given here for clarity:

$$S(\psi) = S_{res} + (S_{sat} - S_{res}) \bullet [1 + (g_a \bullet |\psi|)^{g_n}]^{\left(\frac{1-g_n}{g_n}\right)} \tag{3}$$

$S(\psi)$ is the current degree of saturation, corresponding to the current value of $\psi = -\frac{p_w}{\gamma_w}$, p_w being the suction and γ_w being the unit weight of the pore fluid. S_{sat} and S_{res} are the saturated and residual degrees of saturation, respectively, and g_a and g_n are fitting parameters similar (but not equal) to parameters α and n in the original paper by van Genuchten.[39] The values adopted to reproduce the curve in Fig. 7(a) are summarised in Table 3.

The permeability variation with suction/degree of saturation was not measured experimentally by Kerr et al.[13] Therefore, a variable permeability model, also readily available in PLAXIS 2D, was employed to model the variation of relative permeability, $k_{rel}(S)$, with the effective degree of saturation, S_{eff}:
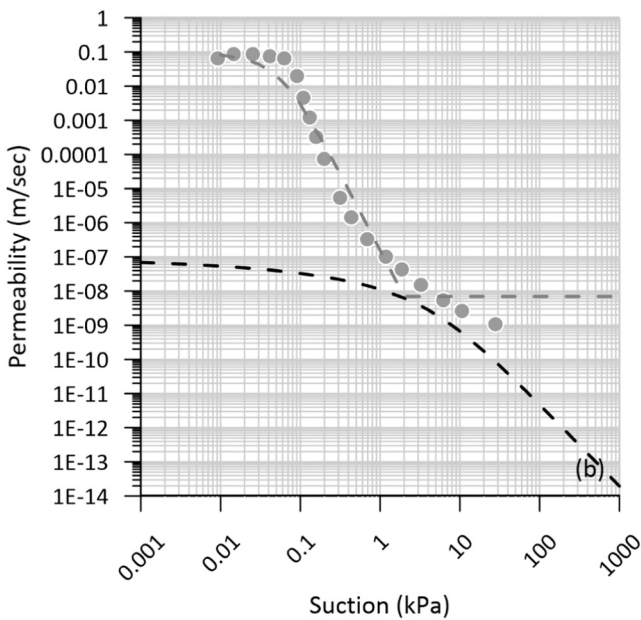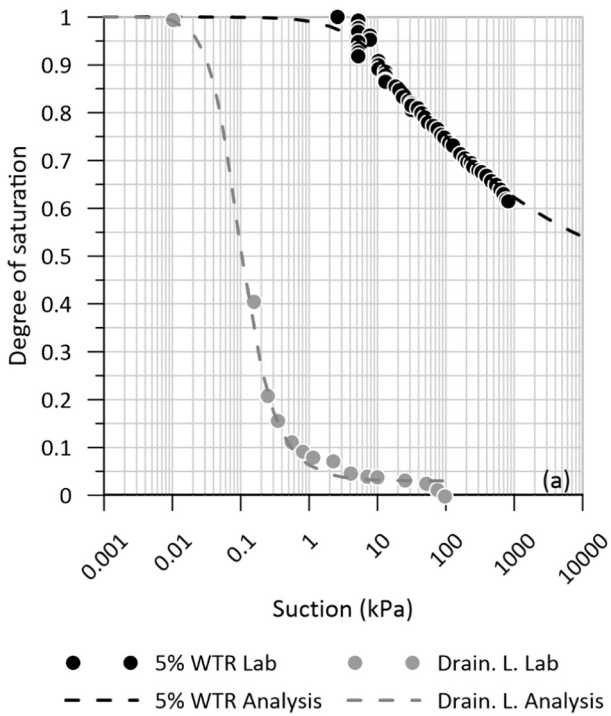
Fig. 8. Vertical displacements with time at the axis of symmetry at different depths before the barrier is constructed.

Fig. 7. Modelling of hydraulic properties of the water holding layer (5% WTR; laboratory data by[13]) and of the drainage layer (Drain. L.; laboratory data by[10]): (a) SWRC; (b) permeability.
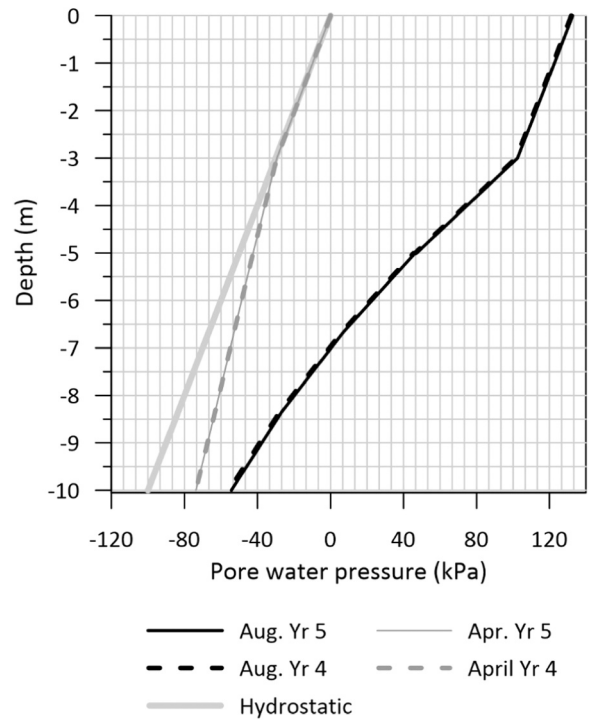
Fig. 9. Pore water pressure profile with depth for August and April of Years 4 and 5.

Table 3
Mechanical and hydraulic parameters for London clay for the water holding layer (5% WTR) and the drainage layer (Drain. L.).

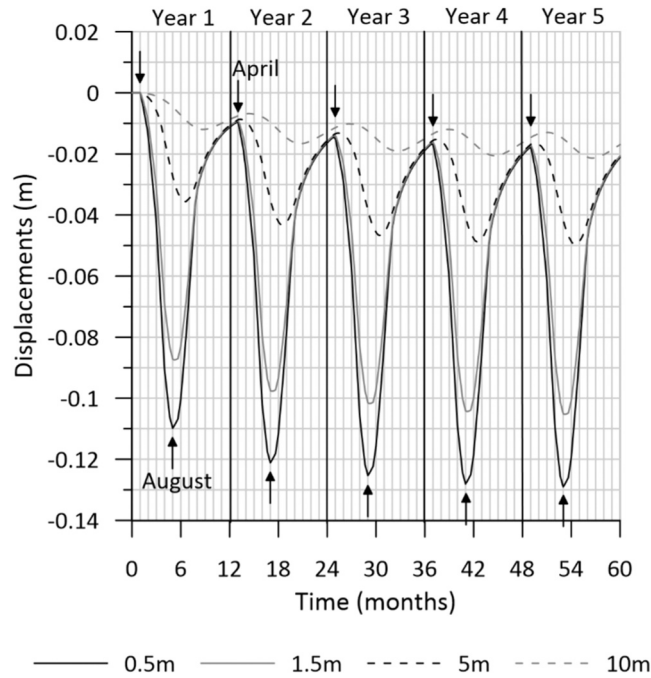| Soil	Young's Modulus (kPa)	Poisson ratio	S_{res}	S_{sat}	g_n	g_a	g_l	k (m/s)
5% WTR	$15 \cdot 10^3$	0.3	0.4	1	1.2	1.4	0	10^{-7}
Drain. L.	$180 \cdot 10^3$	0.2	0.03	1	2.25	1.5	0	10^{-1}
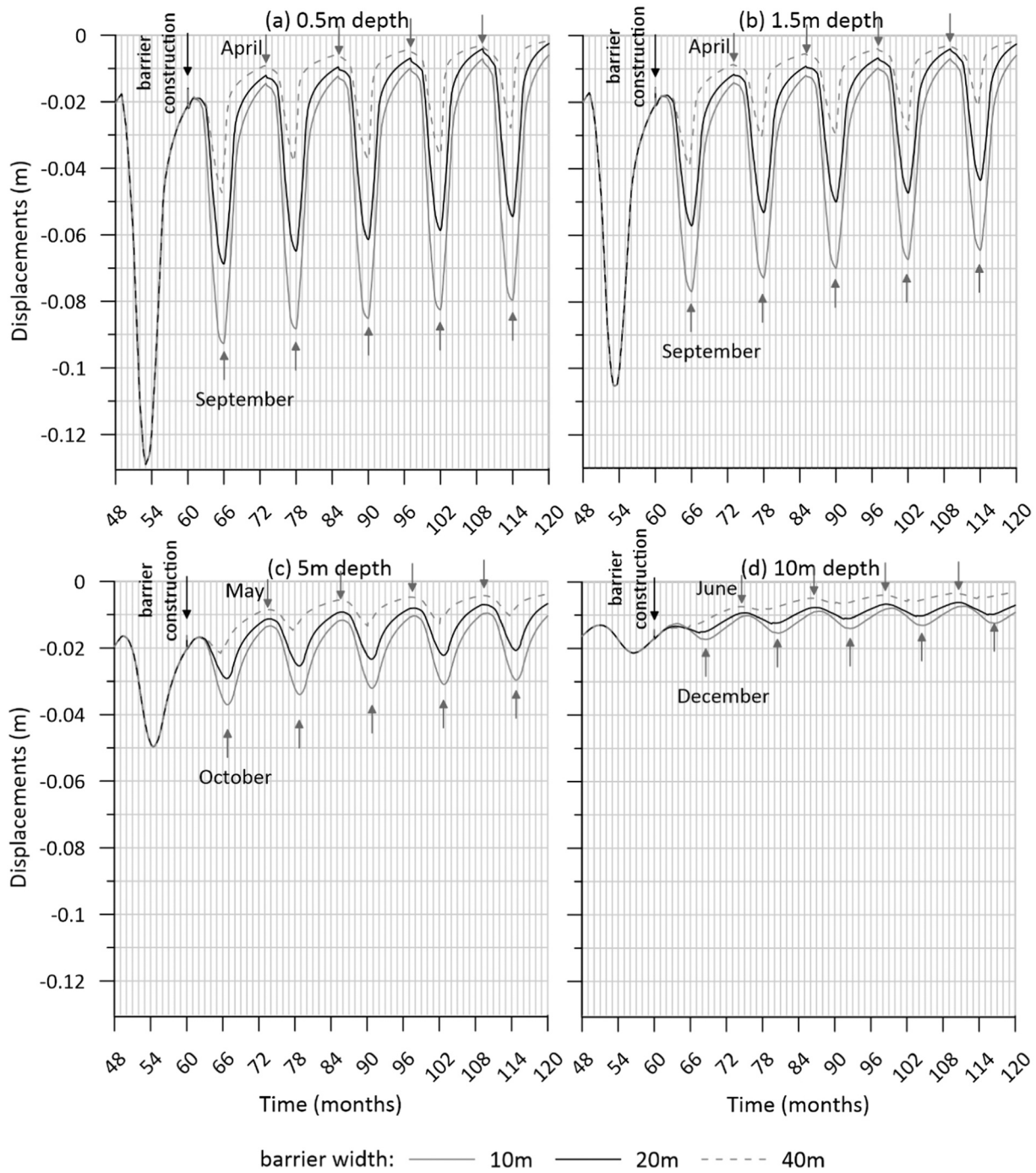
Fig. 10. Effect of barrier width: vertical displacements with time at the axis of symmetry at (a) 0.5 m; (b) 1.5 m; (c) 5 m and (d) 10 m depth for five years after barrier construction and for the final year before barrier construction.

$$S_{eff} = \frac{S(\psi) - S_{res}}{S_{sat} - S_{res}} \quad (4)$$

$$k_{rel}(S) = \left(S_{eff}\right)^{g_l} \bullet \left\{1 - \left[1 - \left(S_{eff}\right)^{\frac{g_n}{g_n-1}}\right]^{\frac{g_n-1}{g_n}}\right\}^2 \quad (5)$$

where g_l is a fitting parameter. The actual isotropic permeability k can be calculated by multiplying the saturated value of permeability by $k_{rel}(S)$. Eq. 3 is similar to the Mualem[18] expression, if $g_l = 1/2$. The value adopted in the analyses is also shown in Table 3. $k_{rel}(S)$ varies between 1 and a minimum value of 10^{-4} set by the program in order to stop the actual permeability from obtaining near zero values, which could cause

numerical non-convergence. The reproduced behaviour is shown in Fig. 7(b).

The drainage layer of the barrier was assumed to be derived from the gravelly sand reported by Indrawan et al.[10] The same SWRC and permeability models as for the water holding layer were used, with the parameters summarised in Table 3. The reproduced behaviour is shown in Fig. 7 and compares very well with the experimentally observed behaviour. Note that a cut-off was used in the model whereby no further changes of permeability were allowed after a suction of 2kPa was reached.

The mechanical behaviour of both layers constituting the barrier was modelled as linear elastic (parameters in Table 3). As the study focused
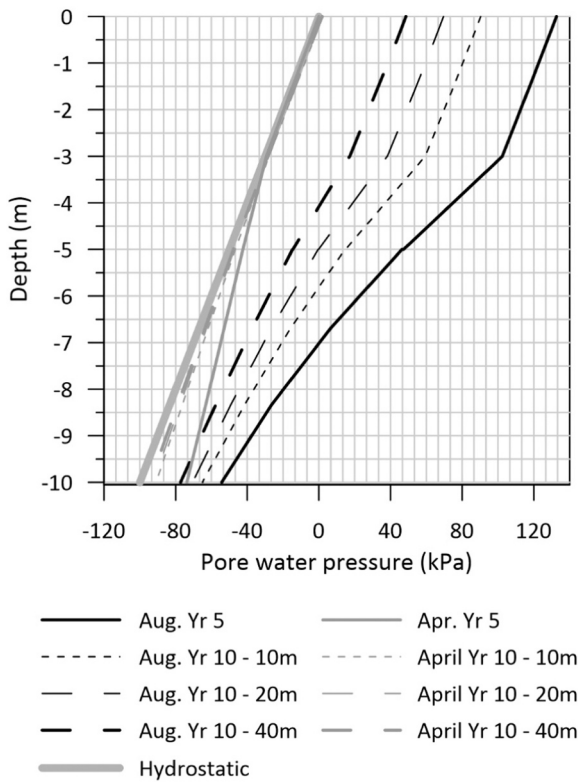
Fig. 11. Pore water pressure profiles with depth at the centre of the barrier, before and after barrier construction, for different barrier width.

on the behaviour of the in-situ soil, this was not considered to be a limitation. The barrier contributes to the in-situ soil displacement with its weight and by affecting the pore water pressures through its hydraulic behaviour, which was accurately captured to the extent that this was possible from the available experimental data.

3. Greenfield condition

3.1. Soil displacements before barrier protection

Fig. 8 presents the evolution of vertical displacements with time predicted by the analysis within the in-situ clay at various depths before the barrier was constructed. Negative displacements signify shrinkage whereas positive displacements signify swelling. The arrows on the figure indicate the end of the dry season at the end of August and the end of the wet season at the end of April. As expected, shrinkage was predicted year after year during the dry period and swelling during the wet period. Swelling in the wet period was smaller than the preceding shrinkage during the previous dry period and overall shrinkage was predicted at the end of each analysis year. The annual shrinkage/swelling increased progressively with time as the pore water pressures deviated from the initial hydrostatic profile (see Fig. 9). As expected, the change in displacements was larger at shallower depths but remained noticeable at 10 m of depth.

The yearly maximum and minimum displacements at 0.5 m and 1.5 m depth coincided with the end of the dry and wet periods respectively, i.e., were obtained at the end of August and end of April. A delayed response to the atmospheric boundary conditions was noticed at 5 m and 10 m depth with yearly minima reached in October and December, and maxima in May and June, respectively. The change from net outflow to net inflow at the beginning of September and vice versa at the beginning of May translated into an abrupt and immediate change from shrinkage to swelling and from swelling to shrinkage, respectively, at 0.5 m and 1.5 m depth but was a lot smoother at 5 and 10 m depth. This is expected, as the pore water pressures react much faster to a change inflow/outflow at the ground boundary at shallower depths.
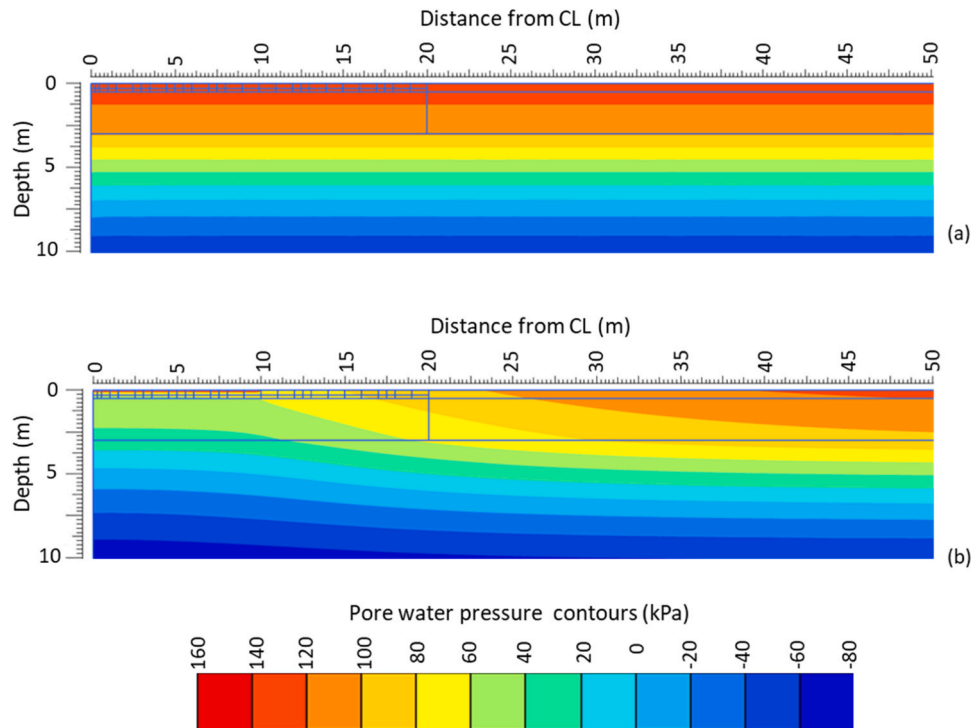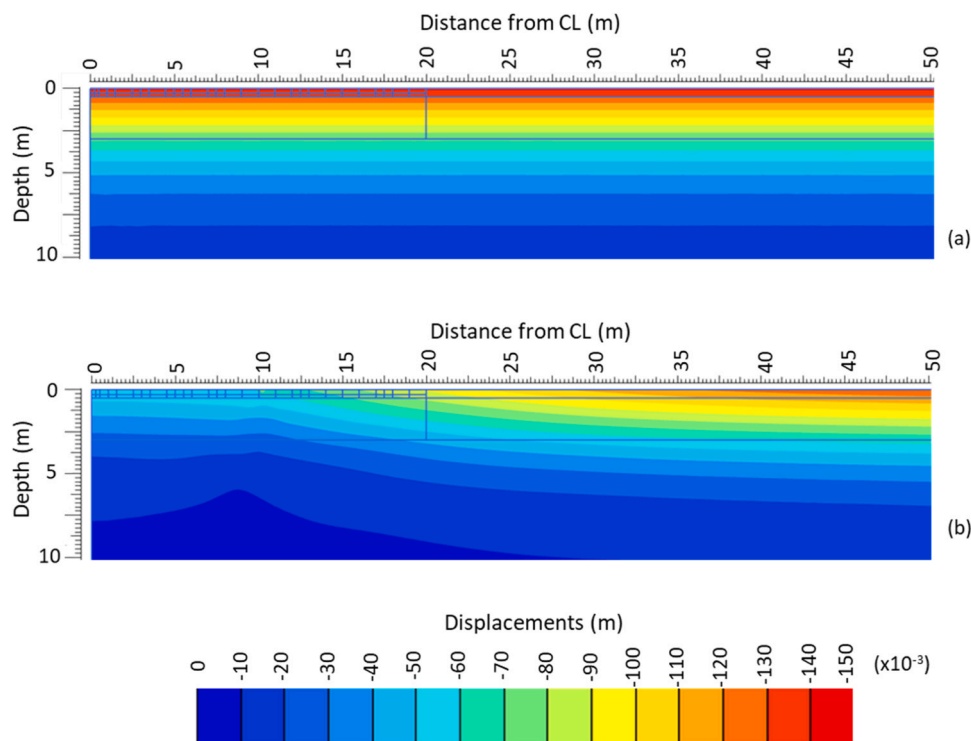

Fig. 12. Contours of pore water pressure profiles for the 20 m wide barrier in August of (a) the final year before barrier construction; (b) the 5th year after barrier construction (suction is positive).

Fig. 13. Contours of vertical displacements for the 20 m wide barrier in August of (a) the final year before barrier construction; (b) the 5th year after barrier construction (negative displacements signify settlement).

It is evident that the annual shrinkage/swelling was significant at shallow depths, where annual changes in the pore water pressure were the largest (see Fig. 9). The net change between yearly maximum and minimum settlement in Year 5 was about 11 cm at 0.5 m depth, and 8.5 cm at 1.5 m depth. This clearly demonstrates a potential problem for shallow buried infrastructure (e.g., pipes, water mains etc.), in particular in the out-of-plane direction at connections with areas covered in impermeable concrete, where there is little interaction with the atmosphere and smaller seasonal ground movements. The seasonal vertical displacement at 5 m depth remained considerable at approximately 3 cm, and reduced to below 1 cm at 10 m depth, demonstrating that the effects of soil-atmosphere interaction can potentially extend deeply into the ground.

3.2. Barrier width

The effect of constructing the barrier on the computed yearly displacements is shown in Fig. 10, which presents the evolution of vertical displacements with time at the same four depths as above, for five years after the barrier was constructed in comparison with the displacements during the final year prior to construction. The time of construction (at 60 months since the start of the analysis) has been marked with an arrow. The different curves correspond to the different widths considered for the barrier: 10, 20 and 40 m. All displacements correspond to the axis of symmetry, i.e., to the centre of the barrier.

Construction of the barrier was beneficial for the seasonal vertical displacements in the in-situ soil in all cases and at all depths, reducing them from about 11 cm at 0.5 m depth prior to the barrier construction to about 7.3, 5 and 3.2 cm after the construction of a 10, 20 and 40 m wide barrier, respectively. At 10 m depth the seasonal vertical displacements were effectively eliminated. The reduction of seasonal vertical displacements was progressive with time, but most of the benefit was seen in the first year with some further – but little and reducing – improvement thereafter. This is a positive outcome, as it demonstrates that the beneficial effect of the barrier can potentially be materialised

within the first year after its construction with some further improvement in subsequent years. The efficacy of engineered barriers as a solution to seasonal movements would be curtailed substantially if benefits would only become visible years after construction.

After the construction of the barrier and independently of its width, the annual maximum displacements were observed in September at 0.5 and 1.5 m depth, instead of August (as before barrier construction). This was the only deviation from the patterns observed before barrier construction. At larger depths the timing of the annual maximum displacement was not affected. The timing of the annual minimum displacements was not affected either at any depth, shallow or deep. With reference to 0.5 and 1.5 m depth, although the change from shrinkage to swelling at the of September remained sharp (as before barrier construction), the change from swelling to shrinkage in April became smoother.

Comparing the effectiveness of the barrier width in reducing soil shrinkage/swelling, it can be observed that the wider the barrier the greater the displacement reduction. This is not surprising, as construction of the barrier altered flow conditions from 1D to 2D through the introduction of the barrier materials, which have different hydraulic properties to the weathered clay they replaced. The effect of this is clearly seen on the pore water pressure profiles with depths plotted in Fig. 11 at the centre of the barrier (i.e., axis of symmetry). The figure illustrates numerical results from the end of August and from the end of April for two different years (the final year before and 5 years after barrier construction, marked respectively as Yr 5 and Yr 10 in the figure) for the three different barrier widths, in comparison to the initial hydrostatic profile. Although there was little difference between the April profiles for the different barriers, the August profiles were substantially different, with the wider barrier yielding the August profile with the smallest deviation from the respective April profile, minimising the seasonal pore water pressure fluctuations and therefore, producing the smallest seasonal vertical displacements. This indicates that a wider barrier contributed to improved lateral isolation of the centre line, where the buried asset would be in this example, from the unmitigated
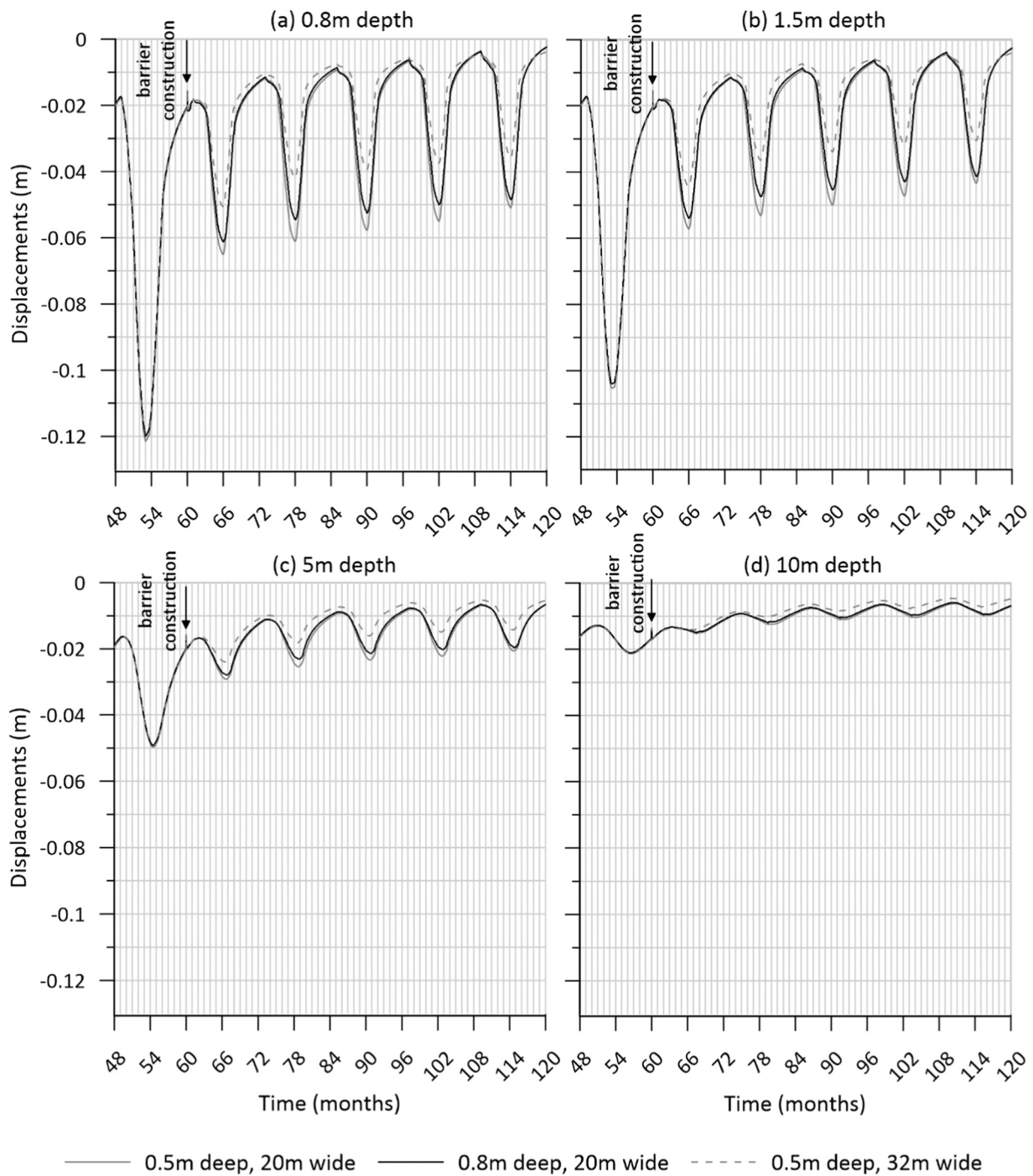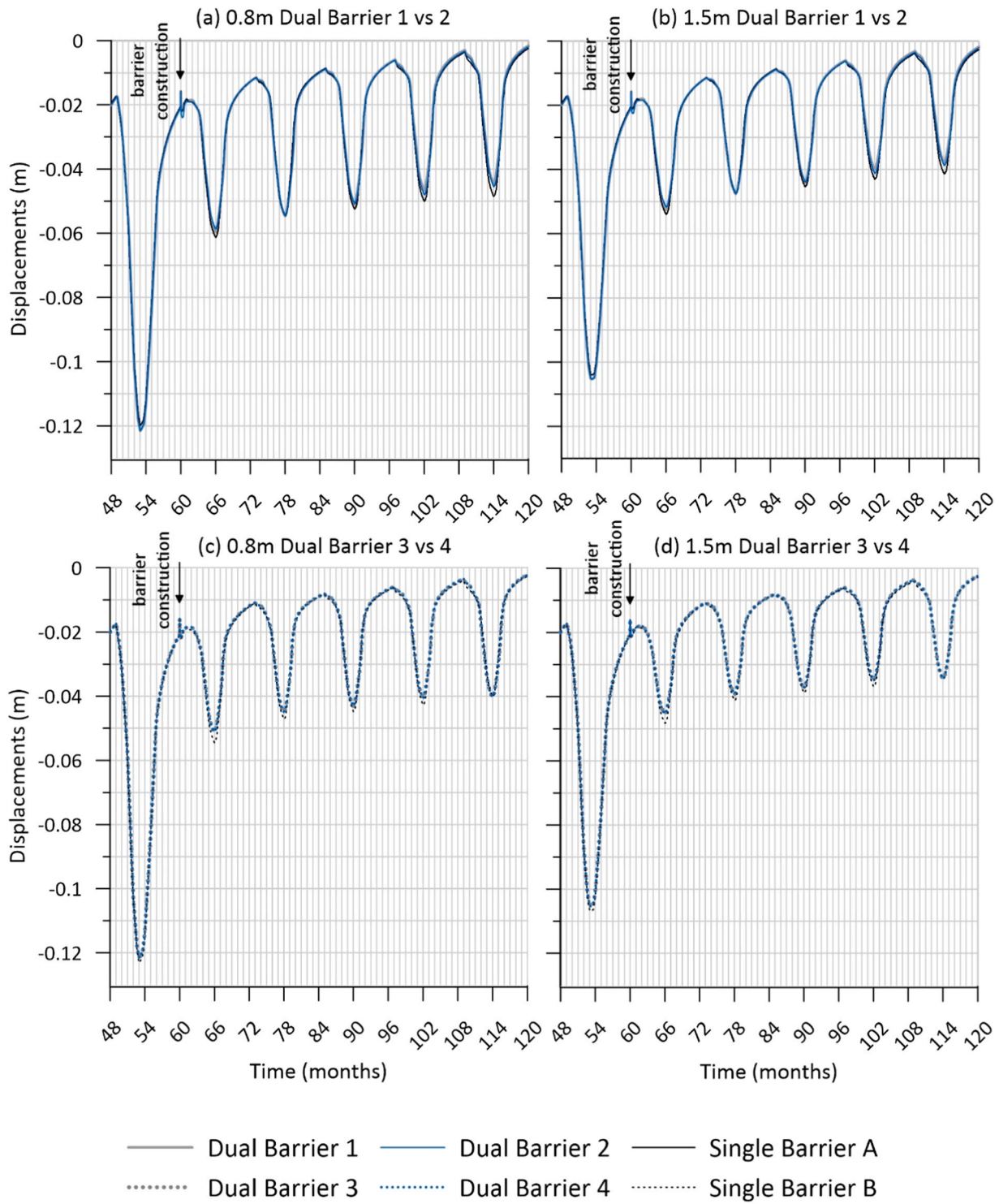
Fig. 14. Effect of barrier depth: vertical displacements with time at the axis of symmetry at (a) 0.8 m; (b) 1.5 m; (c) 5 m and (d) 10 m depth for five years after barrier construction and for the final year before barrier construction.

soil-atmosphere interaction effects.

This is further illustrated in Fig. 12 which shows August pore water pressure contours for the 20 m wide barrier before and 5 years after the construction of the barrier. Although 1D flow conditions before the construction (Fig. 12 (a)) led to uniform horizontal contours, this was no longer the case after construction (Fig. 12 (b)): high suctions were limited to within the barrier itself and did not propagate with depth to the same extent as before the barrier was constructed. The corresponding contours of vertical displacements are shown in Fig. 13.

3.3. Barrier depth

Fig. 14 investigates the effect of the barrier depth for the 20 m wide barrier. The vertical displacements have been plotted at the centre line of the barrier (axis of symmetry) at 1.5, 5 and 10 m as before, and at 0.8 m, to coincide with the depth of the deeper of the two barriers (i.e., excluding the barrier itself and investigating the mechanical behaviour of the underlying in-situ soil). The numerical results demonstrate that increasing the barrier depth had a positive impact on the seasonal vertical displacements up to 5 m depth. The barrier depth made no difference to the displacements at 10 m depth. Overall, the benefit from adopting a deeper layer was small, and it may not outweigh the

Fig. 15. Dual barrier design: vertical displacements with time at the axis of symmetry at (a) 0.8 m and (b) 1.5 m depth for Dual Barriers 1 and 2; (c) 0.8 m and (d) 1.5 m depth for Dual Barriers 3 and 4, in comparison with the corresponding Single Barrier for five years after barrier construction and for the final year before barrier construction.

increased cost of construction (both monetary and environmental).

The dominant effect of width over depth is also demonstrated in Fig. 14, which includes the results of an extra analysis considering a 0.5 m deep/32 m wide barrier, i.e. where the same volume of in-situ soil (16 m^3/m) as in the 0.8 m deep/20 m wide barrier was excavated and replaced. The numerical results indicate that, for a certain volume of excavated soil and constructed barrier (which would be the primary monetary and environmental factor to be taken into account all things

being equal), it would be preferable for the seasonal displacements of the in-situ soil to treat a wider area with a shallower barrier than a narrower area with a deeper barrier. This highlights the potential importance of laterally isolating the buried unfractured from the effects of unmitigated soil-atmosphere interaction, which may be of similar importance to the vertical isolation.
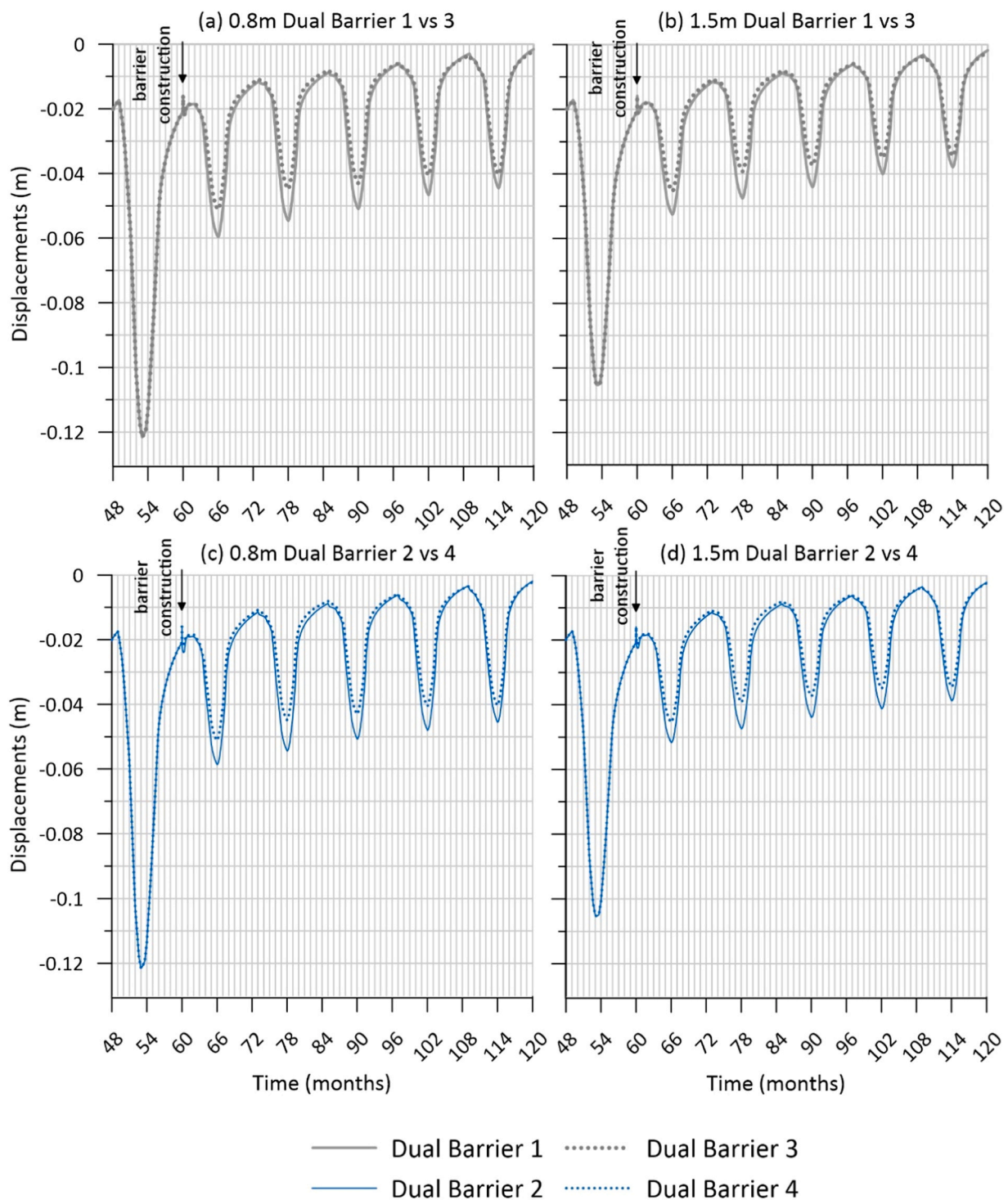
Fig. 16. Dual barrier design: vertical displacements with time at the axis of symmetry at (a) 0.8 m and (b) 1.5 m depth for Dual Barriers 1 and 3; (c) 0.8 m and (d) 1.5 m depth for Dual Barriers 2 and 4 for five years after barrier construction and for the final year before barrier construction.

3.4. Dual barriers

The in-situ vertical displacements calculated at the centre line of the barrier (axis of symmetry) at 0.8 and 1.5 m depth when dual barriers were adopted are illustrated in Fig. 15. Dual Barriers 1 and 2 are compared with the corresponding Single Barrier (A), which had a 0.2 m deep drainage layer, and Dual Barriers 3 and 4 are compared with Single Barrier B, which had a 0.3 m deep drainage layer (i.e., in both cases equal to the total thickness of the two drainage layers of the Dual Barrier, see also Fig. 2). In both comparisons, the Single Barrier performed only slightly worse than the two Dual Barriers, whose results were practically indistinguishable. The configuration of the barrier made very little difference to the results in Fig. 15, meaning that the thickness of the individual water holding layers (top and bottom or single), did not affect the performance of the barrier in reducing the in-situ displacements.

The same results are presented again in Fig. 16 comparing Dual Barriers 1 with 3, and 2 with 4, i.e., dual barriers where the two holding
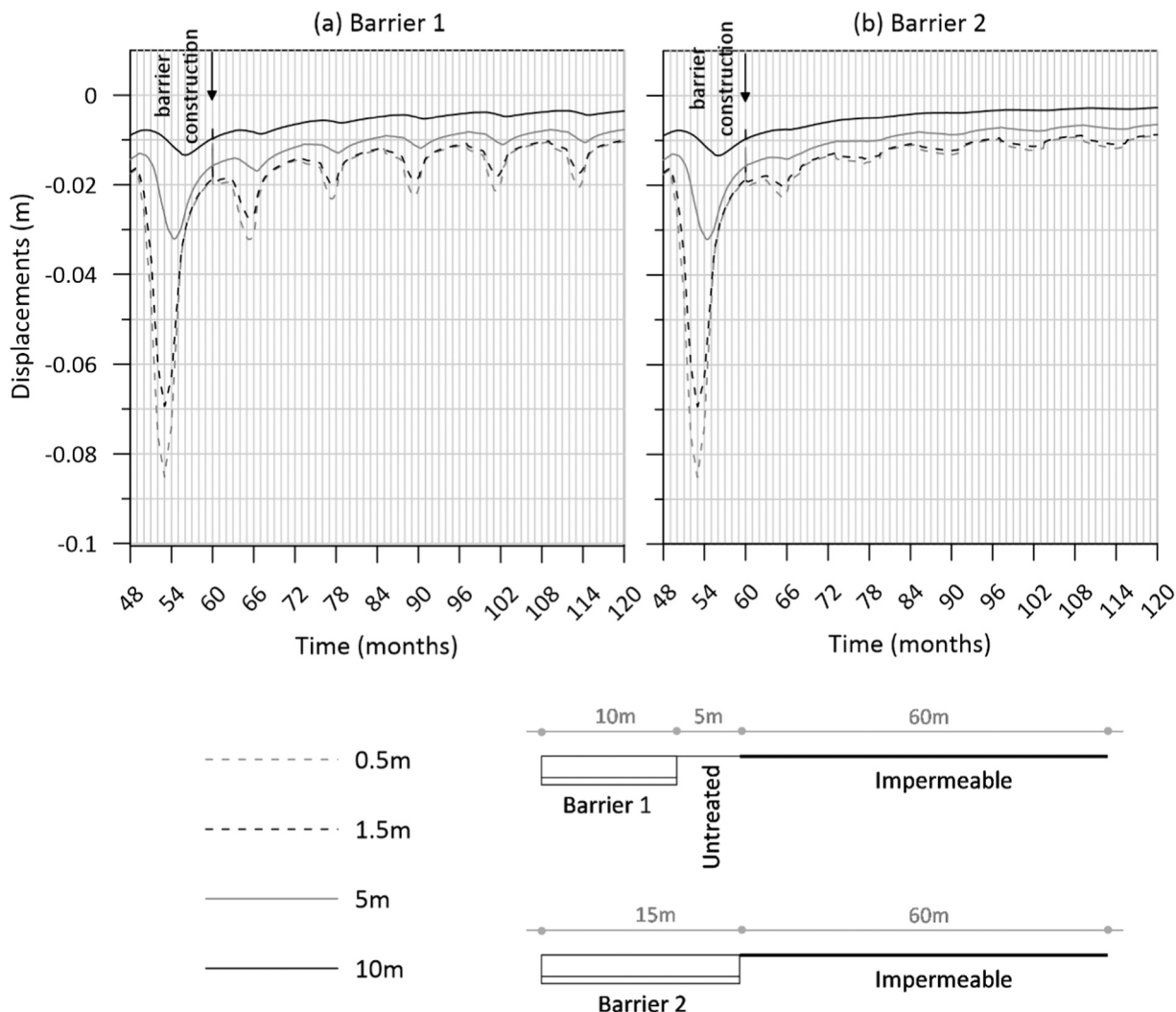
Fig. 17. Barriers close to impermeable boundaries: vertical displacements with time at the axis of symmetry at different depths for (a) 20 m wide barrier (barrier 1); (b) 30 m wide barrier (barrier 2).

layers of each barrier are of either equal (1 and 3) or unequal (2 and 4) thickness (see also Fig. 2). In both comparisons, the dual barrier with the thicker drainage layers (3 and 4) outperformed the corresponding dual barrier with the thinner drainage layers (1 and 2), reducing the in-situ seasonal vertical displacements visibly more.

This is an interesting observation. It indicates that the drainage layer, which acts as a capillary break, plays a major role in reducing displacements. It also indicates that its thickness may be more important than its location within the barrier, as a single layer at its bottom or as a double layer in two vertical locations. This would signify that the water holding layer and the actual design of the barrier (single or double) can potentially be decided based on the design rainfall, while the thickness of the drainage layer which will act as a capillary break can be designed to minimise the displacements in the underlying in-situ soil.

4. Urban conditions

The potential benefit in terms of controlling seasonal vertical displacements in the ground in the proximity of impermeable surfaces in urban environments by engineering appropriate barriers is demonstrated in Fig. 17. The geometries of the two barriers considered are schematically shown in the same figure for ease of refence (see also Fig. 3).

The near-by presence of an impermeable surface had a clear impact,

in relation to the greenfield condition, on the vertical displacements at the axis of symmetry prior to the barrier construction: at 0.5 m depth the seasonal displacement was about 6.5 cm as opposed to 11 cm (see Fig. 10). Similar reductions were observed at larger depths.

The seasonal displacements post-construction were limited to 1 cm at 0.5 m depth, and were virtually eliminated at 10 m in Barrier 1, which left a 5 m strip of untreated soil in between the impermeable surface and the barrier. When the entire area between the axis of symmetry and the impermeable surface was treated (Barrier 2), the seasonal vertical displacements were limited to a few mm and essentially eliminated at all depths within the in-situ soil.

Fig. 18 presents the vertical displacements with time at different depths underneath the impermeable surface, along a vertical which was offset by 5 m from its edge (see also schematic in the same figure). As expected, the vertical displacements prior to the barrier construction were smaller than at the axis of symmetry (see Fig. 17), where the soil fully interacted with the atmosphere. Nonetheless, 5 m within the impermeable surface, the displacements were not zero even at a depth of 10 m, where a few mm of seasonal displacements were obtained. They were as high as 3.7 cm at a depth of 0.5 m. This is due to the changes in pore water pressures underneath the permeable surface that interacted with the atmosphere, and the resulting pore water pressure changes underneath the impermeable surface, arising from the induced 2D flow of water. Contours of suction for August and March before the barrier
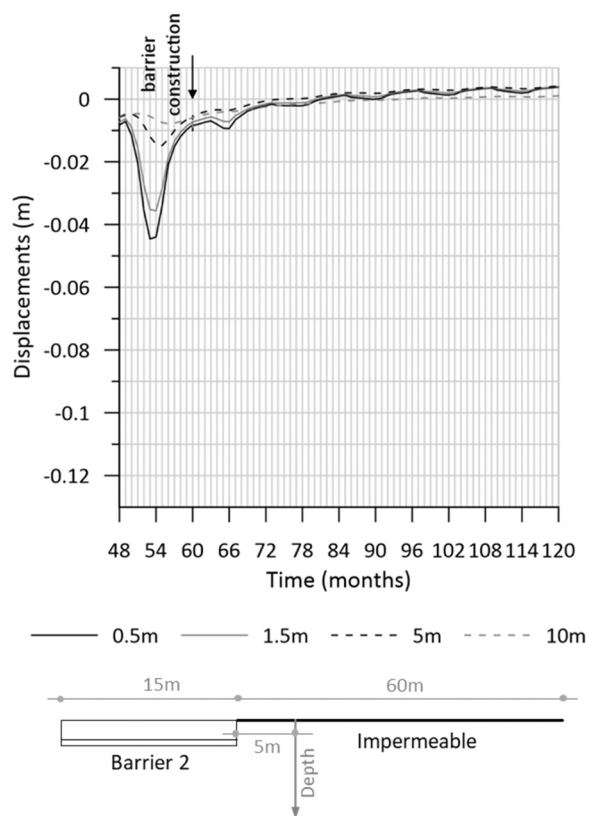
Fig. 18. Barriers close to impermeable boundaries: vertical displacements with time at different depths, at a vertical 5 m offset from the edge of the permeable surface (30 m wide barrier – barrier 2).

construction are presented in Fig. 19 to demonstrate this. In August, high suctions developed where the soil interacted with the atmosphere. Their effect extended horizontally to about 15 m underneath the impermeable surface, and was largest at its edge as expected. In March, suctions were depleted where the soil interacted with the atmosphere, but not entirely lost underneath the impermeable surface, where pore water pressures lagged behind those underneath the permeable surface. Overall, the seasonal fluctuation of pore water pressures was smaller at the vertical line indicated in grey in the figure (for which displacements were reported in Fig. 18) than at the axis of symmetry (for which displacements were reported in Fig. 17).

Following the construction of the barrier, the displacements at 10 m depth returned to zero and showed negligible further seasonal variation (Fig. 18). The seasonal variation of displacements at all other depths was limited to a few mm. The contours of pore water pressures for August of the final year of the analysis were nearly horizontal (Fig. 19 (c)), demonstrating that, as far as the displacements in the in-situ soil are concerned, Barrier 2 isolated it from the atmosphere in a manner almost equivalent to the impermeable surface. It should be noted that this was possible only because the barrier covered the whole of the exposed soil surface (as opposed to Barrier 1, which was seen to be less efficient). It should also be emphasised that suctions as high as 200 kPa developed within the barrier at this point, but the barrier effectively stopped them from propagating within the in-situ soil (Fig. 20). The above demonstrate that engineered barriers can potentially be very effective in urban environments, even when buried infrastructure lies underneath impermeable surfaces.

5. Conclusions

The sets of analyses presented were focused on comparing the

vertical displacements of a plastic clay at selected points and depths, which were induced by the combined effect of rainfall and evapotranspiration, before and after a soil barrier was constructed. The comparison enabled the performance of the soil barrier to be benchmarked and the potential benefits to be explored, clearly providing a proof-of-concept.

The results indicate that the displacements prior to the construction of the barrier can be significant and noticeable at depths possibly extending to 10 m, which can potentially cause serviceability problems for shallow buried infrastructure. Benefits from the construction of the barrier can potentially be materialised within the first year after its construction and can be significant, depending on the width of the barrier. It was found that not only vertical, but also lateral isolation of the points of interest within the ground is important, with wider barriers providing greater reduction in seasonal displacements. The depth of barrier itself, which is of primary significance for flood prevention, has a smaller effect than the width on reducing the seasonal displacements in the underlying soil. Similar conclusions can be drawn for dual capillary break barriers regarding the depth of the water holding layers. It would, therefore, seem reasonable to propose that the thickness of the water holding layer(s) as well as the configuration of the barrier (single or double), should be primarily designed to sustain the selected design rainfall.

The depth of the drainage layer had a significant impact on reducing seasonal displacement. Its location in the case of dual capillary break barriers, made little difference. It would, therefore, follow that, in addition to capillary break and breakthrough, the potential to mitigate shrinkage/swelling should be considered when deciding the thickness of the coarse, drainage layer.

Engineered barriers were shown to be very effective in reducing seasonal displacements not only in greenfield, but also in urban conditions, even when buried infrastructure lies underneath impermeable surfaces, as lateral isolation from the interaction with the atmosphere was also demonstrated to be important. This is an important finding, as the majority of buried infrastructure is naturally concentrated in urban areas. The benefits were maximised when the engineered barrier was extended to connect to impermeable surface.

The conclusions support that it is feasible to engineer soil barriers, not only for flood protection and for preventing percolation of rainfall water to sensitive geo-structures, but also for mitigating the negative effects of seasonal displacement within the ground. The practical potential, therefore, of engineered barriers is manifold. In order to quantify it, collaborative research, combining field, laboratory and numerical studies is necessary. This paper has provided clear evidence that such research would be of great practical value.

CRediT authorship contribution statement

Petalas Alexandros: Conceptualization, Writing – original draft, Writing – review & editing. **Tsiampousi Aikaterini:** Conceptualization, Formal analysis, Investigation, Methodology, Resources, Software, Supervision, Visualization, Writing – original draft, Writing – review & editing. **Day Charlotte:** Formal analysis, Investigation, Methodology, Writing – original draft, Validation.

Declaration of Competing Interest

The authors declare that they have no known competing financial interests or personal relationships that could have appeared to influence the work reported in this paper.

Data availability

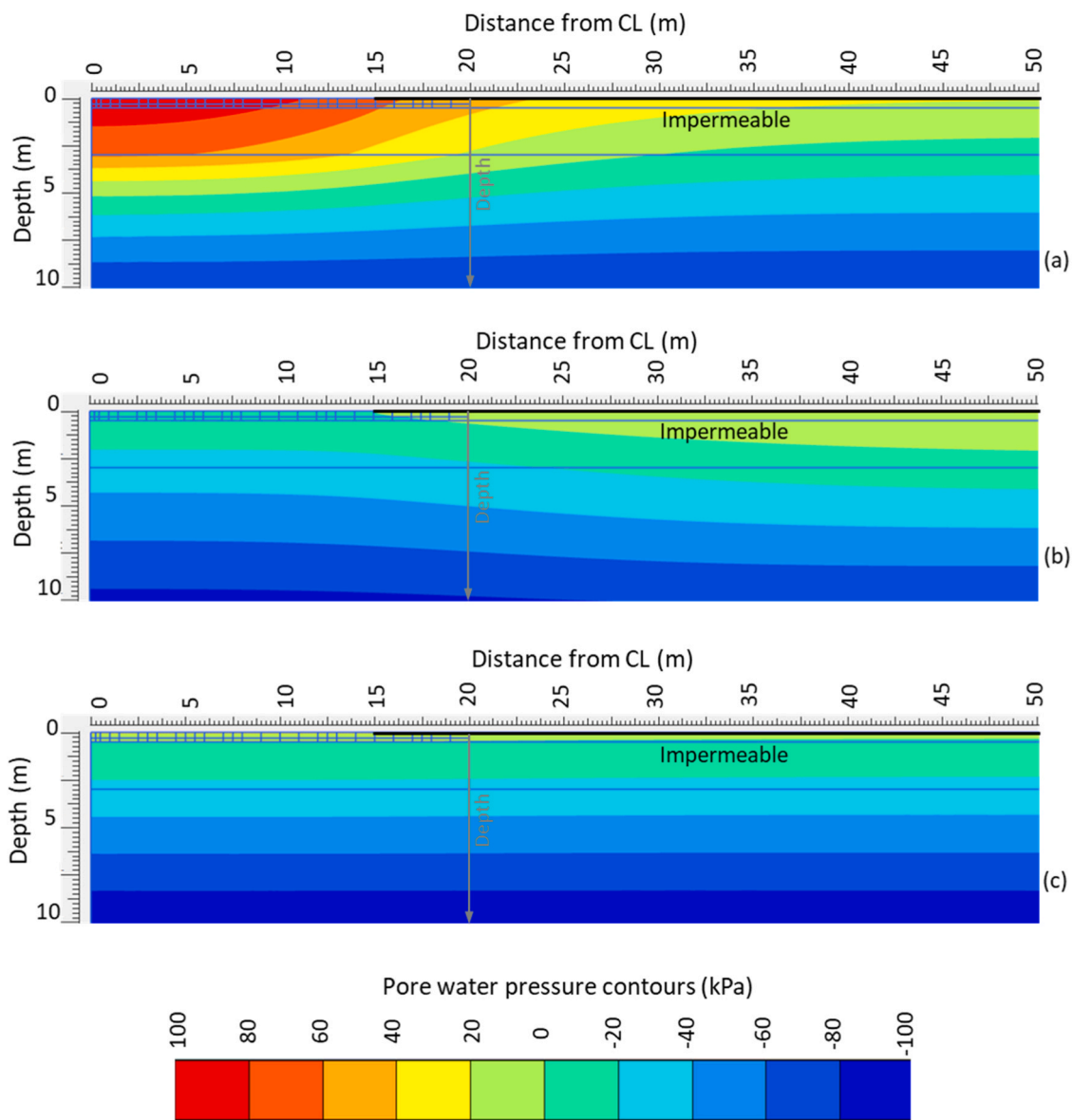Data will be made available on request.

Fig. 19. Contours of pore water pressure profiles for Barrier 2 in (a) August of the final year before barrier construction; (b) March of the final year before barrier construction; (c) August of the 5th year after barrier construction (suction is positive).
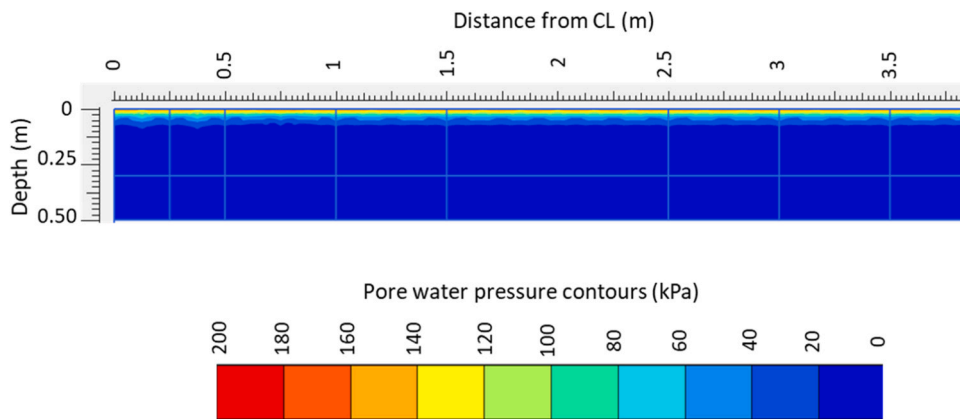

Fig. 20. Contours of pore water pressure profiles for Barrier 2 in August of the 5th year after barrier construction – zoomed-in view (suction is positive).

Appendix A

The constitutive model used to simulate the mechanical behaviour of London clay[33] provides many options with reference to the degradation of shear and bulk stiffnesses with strain which were irrelevant to the analysis: the dependency on void ratio and the dependence of degradation on the stress level (note that the actual stiffness is still stress level dependent, but not its degradation with strain). The equations reported here are simplified from Taborda et al.[33] to reflect those utilised in the analysis.

The tangent shear stiffness, $G_{\tan}$, of the material was calculated as:

$$G_{\tan} = G_{\max} \bullet R_G \tag{S6}$$

where $G_{\max}$ is the maximum tangent shear stiffness and R_G is a reduction factor determined by the deviatoric deformation level. The former was determined as:

$$G_{\max} = G_0 \bullet \left(\frac{p'}{100}\right)^{m_G} \tag{S7}$$

where G_0 is the value of shear stiffness at a reference mean effective stress, p', of 100 kPa (i.e., p'_{ref} was taken as 100 kPa), and m_G is a model parameter controlling the nonlinearity of stress-dependency of the shear modulus. Values for G_0 and m_G have been reported in Table 1. $G_{\max}$ is clearly stress level dependent.

The reduction factor R_G was determined as:

$$R_G = R_{G,\min} + \frac{1 - R_{G,\min}}{1 + \left(\frac{E_d^*}{a_0}\right)^b} \tag{S8}$$

where E_d^* is the deviatoric strain and $R_{G,\min}$, a_0 and b are model parameters (Table 1).

The tangent bulk stiffness, $K_{\tan}$, of the material was calculated as:

$$K_{\tan} = K_{\max} \bullet R_K \tag{S9}$$

where $K_{\max}$ is the maximum tangent bulk stiffness and R_K is a reduction factor determined by the volumetric deformation level. The former was determined as:

$$K_{\max} = K_0 \bullet \left(\frac{p'}{100}\right)^{m_k} \tag{S10}$$

where K_0 is the value of shear stiffness at a reference mean effective stress, p', of 100 kPa (i.e., p'_{ref} was taken as 100 kPa), and m_K is a model parameter controlling the nonlinearity of stress-dependency of the bulk modulus. Values for K_0 and m_K have been reported in Table 1. $K_{\max}$ is clearly stress level dependent.

The reduction factor R_K was determined as:

$$R_K = R_{K,\min} + \frac{1 - R_{K,\min}}{1 + \left(\frac{\varepsilon_{vol}^*}{r_0}\right)^s} \tag{S11}$$

where ε_{vol}^* is the deviatoric strain and $R_{K,\min}$, r_0 and s are model parameters (Table 1).

References

1. Avgerinos V, Potts D, Standing J. The use of kinematic hardening models for predicting tunnelling-induced ground movements in London Clay. *Géotechnique.* 2016;66(2):106–120.
2. Bentley Systems (2022) CONNECT Edition V22.00 PLAXIS 2D Reference Manual.
3. Boldrin D, Knappett JA, Leung KA, Brown JL, et al. Modifying soil properties with herbaceous plants for natural flood risk-reduction. *Ecol Eng.* 2022;180(2022), 106668.
4. Bui, T. A., Casarella, A., Di Donna, A. & Brinkgreve, R. B. J. (2019) Advanced Thermo-Hydro-Mechanical modelling features for practical applications in energy geotechnics, XVII European Conference on Soil Mechanics and Geotechnical Engineering, Reykjavik.
5. Coulombe CE, Wilding LP, Dixon JB. Overview of vertisols: characteristics and impacts on society. *Adv Agron.* 1996;57(1996):289–375. https://doi.org/10.1016/S0065-2113(08)60927-X.
6. Croney D, Coleman J. Soil structure in relation to soil suction. *J Soil Sci.* 1954;5(1): 75–84.
7. Harnas FR, Rahardjo H, Leong EC, Wang JY. An experimental study on dual capillary barrier using recycled asphalt pavement materials. *Can Geotech J.* 2014;51 (10):1165–1177. https://doi.org/10.1139/cgj-2013-0432.
8. Harrison AM, Plim JFM, Harrison M, Jones LD, Culshaw MG. The relationship between shrink–swell occurrence and climate in south-east England. *Proc Geol' Assoc.* 2012;123(4):556–575. https://doi.org/10.1016/j.pgeola.2012.05.002.
9. Hulme M, Turnpenny J, Jenkins GJ. *Climate change scenarios for the United Kingdom: the UKCIP02 briefing report (p. 15)*. Norwich, UK: Tyndall Centre for Climate Change Research, School of Environmental Sciences, University of East Anglia; 2002.
10. Indrawan IGB, Rahardjo H, Leong EC. Drying and wetting characteristics of a two-layer soil column. *Can Geotech J.* 2007;44:20–32. https://doi.org/10.1139/T06-090.
11. Jones LD. *Shrinking and swelling soils in the UK: assessing clays for the planning process.* Earthwise, Issue 18, British Geological Survey; 2002.
12. Jones LD, Jefferson I, Banks V. Swelling and shrinking soils. In: Giles DP, Griffiths JS, eds. *In Geological Hazards in the UK: Their Occurrence, Monitoring and Mitigation. Engineering Geology Special Publications 29.* London, UK: Geological Society; 2020.
13. Kerr HC, Johnson KL, Toll DG. Reusing Fe water treatment residual as a soil amendment to improve physical function and flood resilience. *SOIL Discussions.* 2021:1–23. https://doi.org/10.5194/soil-8-283-2022.
14. Khire MV, Benson CH, Bosscher PJ. Capillary barriers: design variables and water balance. *J Geotech Geonviron Eng.* 2000;126(8):695–708. https://doi.org/10.1061/(ASCE)1090-0241(2000)126:8(695).
15. Kovacevic N, Higgins KG, Potts DM, Vaughan PR. Undrained behaviour of brecciated upper Lias clay at Empingham dam. *Géotechnique.* 2007;57(2):181–195.
16. Li X, Li X, Wang F, Liu Y. The design criterion for capillary barrier cover in multi-climate regions. *Waste Manag.* 2022;149(2022):33–41. https://doi.org/10.1016/j.wasman.2022.06.002.
17. Mair R. Tunnelling and geotechnics: new horizons. *Géotechnique.* 2008;58(9): 695–736.
18. Mualem Y. A new model for predicting the hydraulic conductivity of unsaturated porous media. *Water Resour.* 1976;12(3):513–522.
19. Nelson JD, Miller DJ. *Expansive soils.* New York: Wiley,; 1992.
20. Nyambayo VP. *Numerical analysis of evapotranspiration and its influence on embankments. PhD Thesis. Imperial College.* UK: University of London; 2003.
21. Nyambayo VP, Potts DM. Numerical simulation of evapotranspiration using a root water uptake model. *Comput Geotech.* 2010;37:175–186.
22. O'Brien AS. "The assessment of old railway embankments: Time for a change?". *Partial Satur Compact Soil: Geotech Symp Print 2011.* 2013:19–32.

23. Parent SE, Cabral A. Material selection for the design of inclined covers with capillary barrier effect (et al.). In: Alshawabkeh A, Benson CH, Culligan PJ, Evans JC, eds. *Proceedings of Geo-Frontiers 2005*. Austin: ASCE; 2005:1–5 (et al.).

24. Petalas AL, Tsiampousi A, Zdravkovic L, Potts DM. Numerical investigation of the performance of engineered barriers in controlling stormwater runoff (In press) *Geomech Energy Environ*. 2022. https://doi.org/10.1016/j.gete.2022.100401.

25. Pugh RS. Some observations on the influence of recent climate change on the subsidence of shallow foundations. *Geotech Eng*. 2002;155(1):23–25. https://doi.org/10.1680/geng.2002.155.1.23.

26. Rana A, Sharma A, Kumar A, Azizi A, et al. *An Apparatus to Monitor Suction Evolution and Water Migration within a Soil Mass for Climate-Adaptive Infrastructure*. IIT Mandi; 2022.

27. Scarfone R, Wheeler SJ, Smith C. Numerical modelling of the application of capillary barrier systems for prevention of rainfall-induced slope instability. *Acta Geotech*. 2022;18(7):355–378. https://doi.org/10.1007/s11440-022-01582-w.

28. Smesrud JK, Selker JS. Effect of Soil-Particle Size Contrast on Capillary Barrier Performance. *J Geotech Geoenviron Eng*. 2001;127(10):885–888. https://doi.org/10.1061/(ASCE)1090-0241(2001)127:10(885).

29. Smethurst JA, Clarke D, Powrie W. *Seasonal changes in pore water pressure in a grass-covered cut slope in London Clay. Stiff Sedimentary Clays: Genesis and Engineering Behaviour: Géotechnique Symposium in Print 2007*. Thomas Telford Ltd.; 2011: 337–351. https://doi.org/10.1680/geot.10.P.097.

30. Taborda D, Potts D, Zdravkovic L. On the assessment of energy dissipated through hysteresis in finite element analysis. *Comput Geotech*. 2016;71:180–194.

31. Taborda DMG, Tsiampousi A, Kontoe S. IC MAGE Flow Model 02 – stress-dependent anisotropic permeability (1.0). *Zenodo*. 2023. https://doi.org/10.5281/zenodo.7803819.

32. Taborda DMG, Kontoe S, Tsiampousi A. IC MAGE UMIP – universal model interface for PLAXIS (Version 3.3). *Zenodo*. 2023. https://doi.org/10.5281/zenodo.7564989.

33. Taborda DMG, Kontoe S, Tsiampousi A. "IC MAGE Model 01 – strain hardening/softening Mohr-Coulomb failure criterion with isotropic small strain stiffness (Version 2.0)". *Zenodo*. 2023. https://doi.org/10.5281/zenodo.7565062.

34. Toll, D.G., Kerr, H., Hughes, P.N., Johnson, K.L. et al. (2021) Investigating Water Holding Barriers for Climate Adaptation. In: CACTUS. 20th International Conference on Soil Mechanics and Geotechnical Engineering. Sydney, Australia. Pp. 1–6.

35. Tsiampousi A. 3D effects of soil-atmosphere interaction on infrastructure slope stability. *Proc 8th Int Conf Unsatur Soils*. 2023.

36. Tsiampousi A, Zdravkovic L, Potts D. Numerical study of the effects of soil-atmosphere interaction on the stability and serviceability of cut slopes in London clay. *Can Geotech J*. 2017;54:405–418.

37. Tsiampousi A, Taborda DMG, Kontoe S. IC MAGE Flow Model 04 – anisotropic permeability model for simulating desiccation (1.0). *Zenodo*. 2023. https://doi.org/10.5281/zenodo.8413267.

38. United Nations. (2018) The World's Cities in 2018. UN.

39. van Genuchten MT. A closed-form equation for predicting the hydraulic conductivity of unsaturated soils. *Soil Sci Soc Am J*. 1980;44(5):892–898.

40. Wongsaroj J, Soga K, Mair R. Tunnelling-induced consolidation settlements in London Clay. *Géotechnique*. 2013;63(13):1103–1115.

41. Yang H, Rahardjo H, Leong E, Fredlund DG. Factors affecting drying and wetting soil-water characteristic curves of sandy soils. *Can Geotech J*. 2004;41(5):908–920. https://doi.org/10.1139/t04-042.